

Electronic Supplementary Information

Polyaniline nanowires dotted on graphene oxide nanosheets as a novel super adsorbent for Cr(VI)

Shouwei Zhang^{a,b}, Wenqing Xu^c, Jiaying Li^{*a}, Jie Li^a, Jinzhang Xu^b, Xiangke Wang^a

^a *Key Laboratory of Novel Thin Film Solar Cells, Institute of Plasma Physics, Chinese Academy of Sciences, 230031, Hefei, PR China. Fax: +86-551-559-1310; Tel: +86-551-55-2788; E-mail: lijx@ipp.ac.cn*

^b *School of Material Science and Engineering, Hefei University of Technology, Hefei 230031, China*

^c *Department of Chemical Engineering, Environmental Engineering Program, Yale University New Haven, Connecticut 06520*

1. Experimental details

1.1 Preparation of water-soluble, few-layered graphene oxide (GO) nanosheets.

Graphene oxide was prepared using modified Hummers method from flake graphite (average particle diameter of 4 μm , 99.95% purity, Qingdao Tianhe Graphite Co. Ltd., Qingdao, China). Briefly, 5 g of graphite and 3.75 g of NaNO_3 (A.R.) were placed in a flask. Then, 375 mL of H_2SO_4 (A.R.) was added with stirring in an ice-water bath, and 22.5 g of KMnO_4 (A.R.) were slowly added over about 2 h. Stirring was continued for 2 h in the ice-water bath. After the mixture was stirred vigorously for 5 days at room temperature, 700 mL of 5 wt.% H_2SO_4 aqueous solution was added over about 1 h with stirring, and the temperature was kept at 98 °C. The resultant mixture was further stirred for 2 h at 98 °C. When the temperature was reduced to 60 °C, 15 mL of H_2O_2 (30 wt.% aqueous solution) was added, and the mixture was stirred for 2 h at room temperature.

To remove the ions of oxidant and other inorganic impurity, the resultant mixture was purified by repeating the following procedure cycle 15 times: centrifugation, removal of the supernatant liquid, addition of 2 L of a mixed aqueous solution of 3 wt.% H_2SO_4 /0.5 wt.% H_2O_2 to the bottom solid, and dispersing the solid using vigorous stirring and bath ultrasonication for 30 min at a power of 140 W. Then a similar procedure was repeated: three times using 3 wt.% HCl aqueous solution (2 L) and one time using H_2O (2 L). The final resultant water solution was centrifuged, and then sample was rinsed with Milli-Q water until the solution was neutral. The desired products were dried in a vacuum tank at room temperature.

1.2 Preparation of PANI/GO nanocomposites.

PANI/GO nanocomposites were synthesized by dilute polymerization in the presence of GO and aniline monomer. In a typical procedure, 15 mL GO aqueous solution (containing 100 mg of GO) was added into 160 mL of 1 mol/L HClO_4 ethanol solution, and the mixture was ultrasonicated until GO was fully dispersed. Then aniline monomer was added into the above solution and stirred for 30 min at $-20\text{ }^\circ\text{C}$ to form a uniform mixture. The oxidant, $(\text{NH}_4)_2\text{S}_2\text{O}_8$ (APS) was dissolved in 40 mL of HClO_4 ethanol solution (the molar ratio of aniline/APS is 1.5) and cooled to $-20\text{ }^\circ\text{C}$. The polymerization was performed by rapid addition of the pre-cooled oxidant solution, and the mixture was stirred for 24 h at $-20\text{ }^\circ\text{C}$. Finally, the black green precipitates were filtered and washed with a large amount of water and ethanol. The samples were dried at $60\text{ }^\circ\text{C}$ for 24 h under vacuum. For comparison, random

connected PANI nanowires were synthesized chemically at 0.05 mol/L aniline in the absence of GO via the similar procedure above.

2. Sample Characterization

The crystal structures were analyzed by X-ray powder diffraction (XRD, X'Pert PRO) equipped with Cu K α radiation ($\lambda=0.15406$ nm). Fourier Transforms Infrared spectroscopy (FT-IR) was carried out on a Bruker EQUINOX55 spectrometer (Nexus) in KBr pellet at room temperature. X-ray photoelectron spectroscopy (XPS) spectrum was recorded with a Thermo VG Scientific Sigma Probe spectrometer. The morphologies of PANI/GO were observed by a field-emission scanning electron microscope (FE-SEM, Sirion 200). Transmission electron microscopy (TEM) images was taken on a TECNAI F20 (Philips) at 200kV. Raman spectra were recorded using a micro-Raman spectroscopy (JY-HR800, the excitation wavelength at 532 nm). Thermogravimetric analysis was performed with a NETZSCH TG209 F3 instrument under a 20 mL/min N₂ at the heating rate of 20 °C/min.

3. Application of prepared PANI/GO nanocomposite for Cr(VI) removal

PANI/GO stock suspensions were prepared by ultrasonication of 0.1 g PANI/GO nanocomposites in Milli-Q water to achieve the concentration of 0.2 g/L. The stock solution of Cr(VI) was prepared by dissolving the solid potassium dichromate (K₂Cr₂O₇) to Milli-Q water. For Cr(VI) adsorption, PANI/GO suspensions and Cr(VI) solutions were added to 10 mL polyethylene tubes to achieve the desired

concentrations of different components. The pH was adjusted to 3 by adding negligible volumes of 0.01 or 0.1 M NaOH or HCl. After the mixture was oscillated for 24 h, the solid and liquid phases were separated by centrifugation at 9800 rpm for 20 min. The concentration of Cr(VI) in the supernatant was determined with ICP-MS. The removal percentage (%) and amounts of Cr(VI) adsorbed on solid phase (q_e) were calculated from the concentration difference between the initial concentration (C_0) and the equilibrium one (C_e):

$$\text{Removal}(\%) = \frac{C_0 - C_e}{C_0} \times 100\%$$

$$q_e = \frac{(C_0 - C_e) \times V}{m}$$

where C_0 is the initial concentration (mg/L), C_e is the equilibrium concentration (mg/L), q_e is the amount of Cr(VI) adsorbed on PANI/GO at equilibrium time (mg/g), V is the solution volume (L), and m is the mass of the adsorbent (g).

Characterization information

In the XRD patterns (Fig. S1a) of GO and graphite, the diffraction peak at $2\theta = 26.41^\circ$ ($d = 0.34$ nm) corresponding to the normal graphite spacing (002) of the graphite plane, disappeared in the synthesized graphene oxide in the oxidation process. The broad and relatively weak diffraction peak at $2\theta = 10.03^\circ$ with $d = 0.87$ nm corresponding to the typical diffraction peak of GO is attributed to the (002) plane. The c-axis spacing increases from 0.34 to 0.87 nm after the graphite is modified to GO nanosheets during the oxidation process, which may be due to the creation of the oxygen-containing functional groups on GO, and the functional groups are evidenced by the following

XPS analysis. As shown in Fig. S1b, the C1s XPS spectrum of GO indicates a considerable degree of oxidation with different functional groups: the nonoxygenated ring C (284.5 eV), the C atom in C-O bond (286.2 eV), the carbonyl C (287.8 eV), and the carboxylate carbon (O-C=O) (289.0 eV). The relative contents of different functional groups from the curve fitting of the C1s XPS spectrum are showed in Fig. S1b. The ratio of carbon to oxygen (C/O) is about 2.37 in the graphene oxide, which indicates the high oxidation of the synthesized GO by the oxidant. The specific peak area shows that the main oxygen-containing groups are C-O and C=O, which are expected to form strong surface complexes with aniline on the surfaces of GO. The Raman spectrum of GO is shown in Fig. S1c. The obvious bands at around 1580 and 1350 cm^{-1} are generally assigned as the G band (associated with the vibration of sp^2 carbon atoms in a graphitic 2D hexagonal lattice) and D band (related to the vibrations of sp^3 carbon atoms of defects and disorder). The G band is associated with the vibration of sp^2 carbon atoms in a graphitic 2D hexagonal lattice, and the D band at around 1350 cm^{-1} is related to the vibrations of sp^3 carbon atoms of defects and disorder. The weak and broad 2D peak at 2700 cm^{-1} is another indication of disorder due to an out of plane vibrational mode, and the cooperation between D and G peaks also gives rise to an S3 peak near 2950 cm^{-1} . The synthesized GO also has very high dispersion properties in aqueous solutions. The GO suspension did not form any aggregation even after 5 months of aging time, and had a brown yellow color (Fig. S1d). The good dispersion properties of GO in aqueous solution are attributed to a lot of oxygen containing functional groups on the surface of GO nanosheets, which not

only make GO nanosheets easily disperse in aqueous solution but also may act as the nucleation sites for PANI decoration.

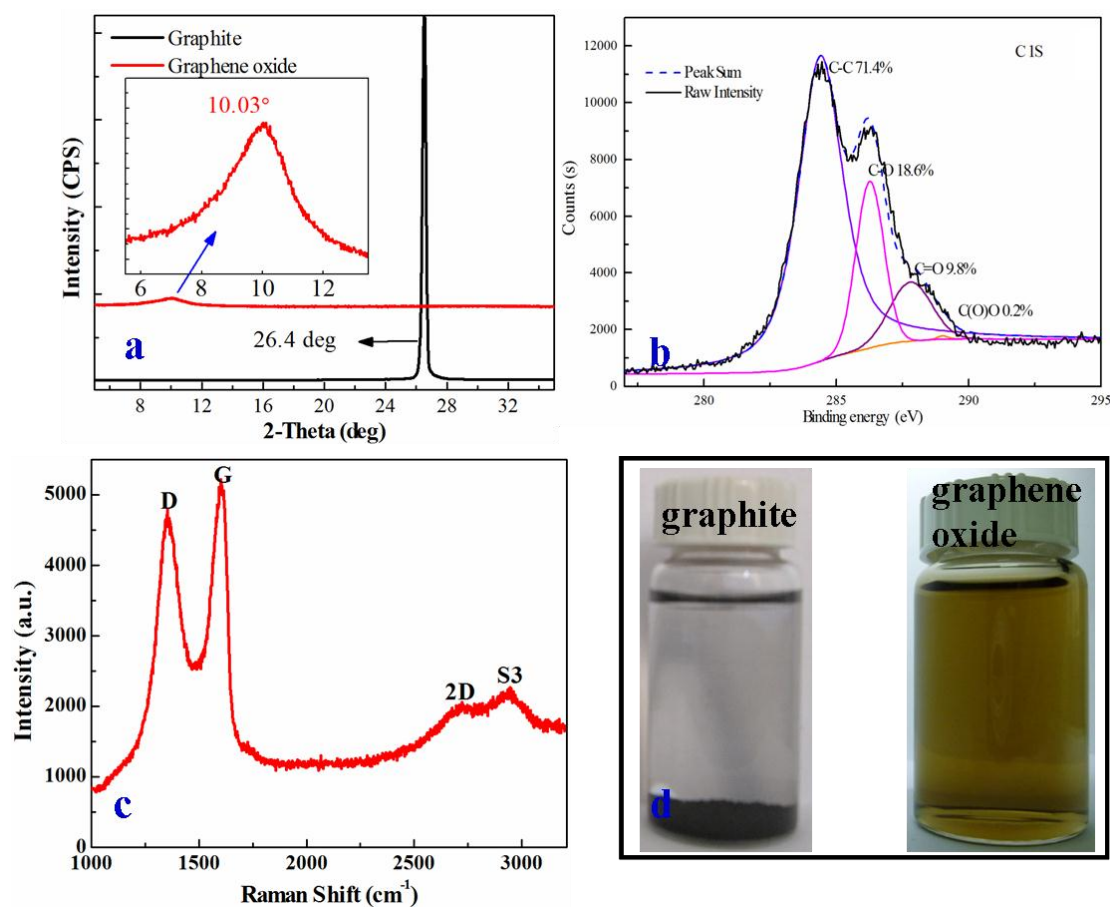


Figure S1: (a) X-ray diffraction of GO and graphite, (b) C1s spectra of GO, (c) Raman spectra of GO, and (d) Aqueous solution of GO (0.5 mg/mL) and graphite (0.5 mg/mL).

In order to further understand the changes in the morphology and the formation mechanism of the hierarchical nanocomposites, PANI/GO nanocomposites were taken out from the reaction solution at different time intervals during the polymerization process and were monitored by FE-SEM. As displayed in Fig. S2b, GO nanosheets still looked smooth after 1.5 h polymerization, but the GO nanosheets become thick

obviously. A few tiny protuberances were formed on the surface of GO after a reaction time of 2.5 h (Fig. S2c), which were different from the smooth surface of the pure GO. The number and size of the protuberances increases with the average length being ~25 nm after reaction time 7.5 h (Fig. S2d). When the polymerization time extends to 12 h, the length of the PANI protuberances increases further with the average size increasing to about 40 nm (Fig. S2e). Finally, about 50 nm aligned PANI nanowires are formed vertically along the surface of the GO (Fig. S2f). GO nanosheets have two-dimensional sheets that have various oxygen functional groups (e.g., hydroxyl, epoxy, and carbonyl groups) on their basal planes and edges. These functional groups act as anchor sites for aniline and enable the subsequent in situ polymerization of PANI attaching on the surfaces and edges of GO nanosheets. Besides, the π - π stacking force between the phenyl and basal planes of GO was also beneficial to in situ polymerization occurring on the surface of GO.

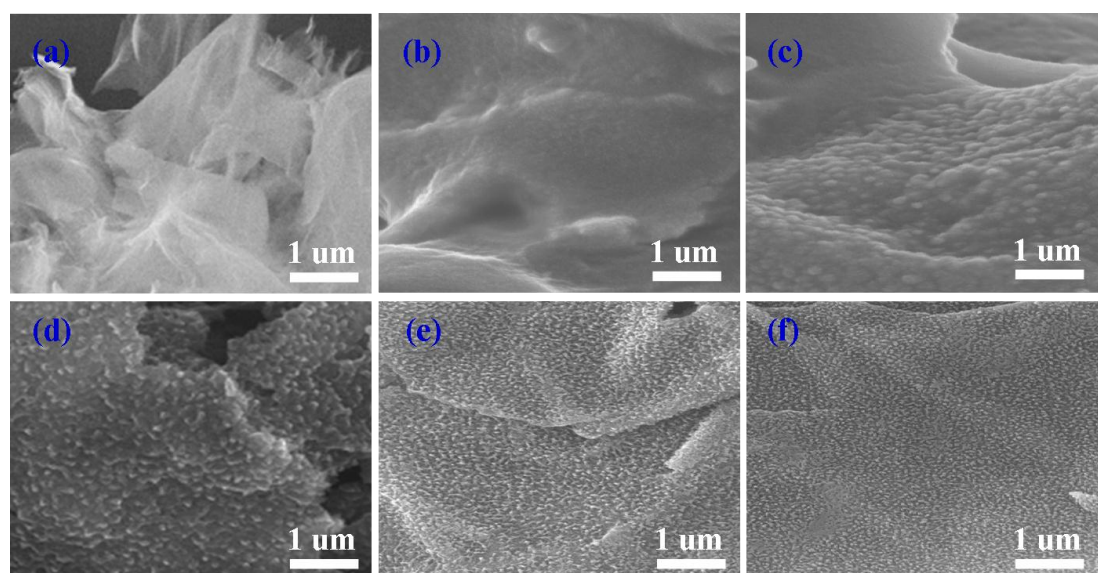


Figure S2. FE-SEM images of PANI/GO nanocomposites synthesized at different polymerization time: (a) 0 h, (b) 1.5 h, (c) 2.5 h, (d) 7.5 h, (e) 12 h, (f) 24 h.

In addition, the thickness of the PANI shell in PANI/GO composites is readily tunable by simply adjusting the mass ratio of aniline to GO in the fabrication process and, as a consequence, the removal ability of heavy metal ions by the PANI/GO shows a dependence on the thickness of the PANI coating shell or the ratio of aniline to GO. As shown in Fig. S3, the thickness of the obtained PANI/GO is ~ 40 nm when the mass ratio of aniline to GO is 2.2 : 1. Thus, the thickness of the PANI coating shell is about 20 nm because the graphene core is very thin (~ 1.0 nm). When the mass ratio of aniline to GO is increased from 4.6 : 1 to 9.3 : 1, the thickness of the PANI coating shell is increased from ~ 45 nm to ~ 80 nm (see Figs. S3b and S3c). But free PANI particles appear when the mass ratio of aniline to GO is further increased to 13.5 : 1 due to the homogeneous nucleation of the excess aniline monomer. The removal ability of the PANI/GO suspension is found to be the highest when the mass ratio of aniline to GO is about 9.3 : 1 (see Fig. S4). The PANI coating shell is too thin to prevent the restacking between the GO nanosheets. However, when the thickness of the PANI coating shell is too thick or the mass ratio of aniline to GO is too high, the decrease of the removal ability may be attributed that the GO was completely covered by PANI nanowires. The experimental results clearly show that the mass ratio of aniline to GO has an obvious effect on the morphology of the PANI/GO composites, and also confirm the formation mechanism proposed above.

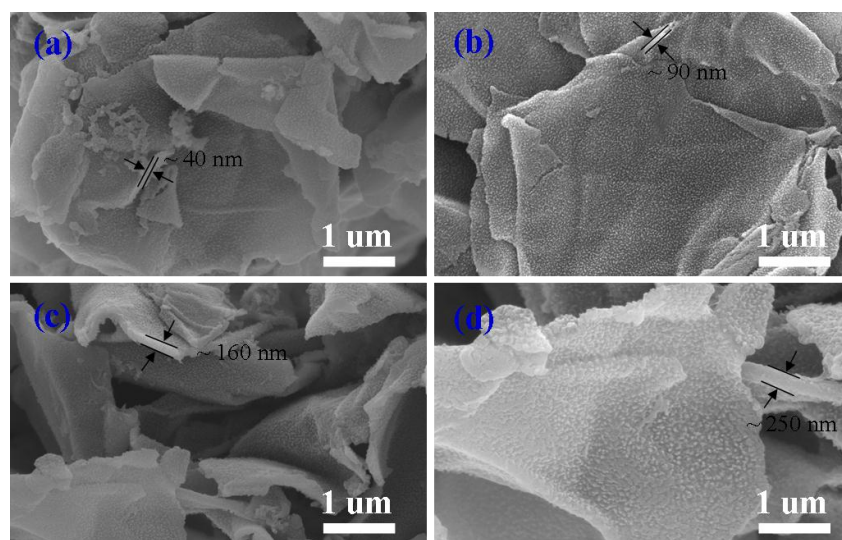


Figure S3. SEM images of PANI/GO nanocomposites synthesized by different mass ratio of aniline to GO: (a) aniline:GO =2.2:1, (b) aniline:GO =4.6:1, (c) aniline:GO =9.3:1, (d) aniline:GO =13.5:1. Because the graphene core is very thin (~1 nm), the thickness of PANI coating shell is ~20 nm for (a), ~45 nm for (b), ~80 nm for (c), and ~125 nm for (d).

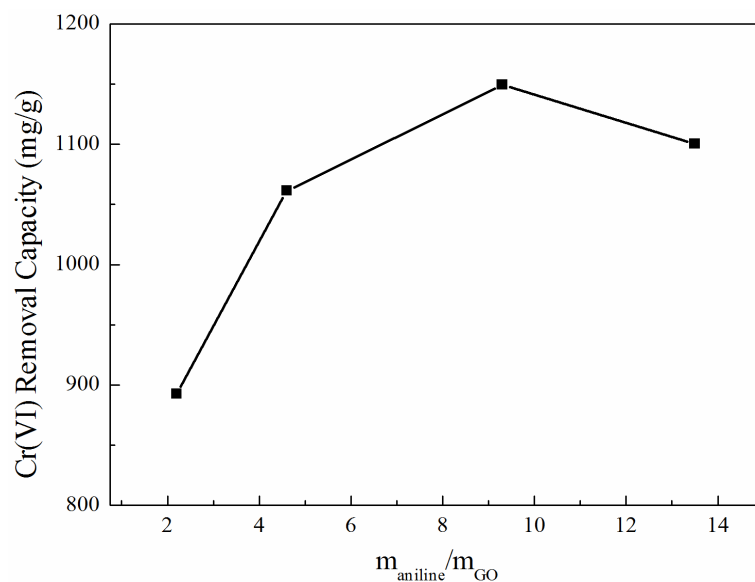


Figure S4. The Cr(VI) removal capacity by PANI/GO nanocomposites synthesized by different mass ratio of aniline to GO.

The Langmuir and Freundlich isotherm models are applied to simulate Cr(VI) adsorption on PANI/GO composites. The Langmuir model is expressed as:

$$q_e = \frac{bq_m C_e}{1 + bC_e}$$

The Freundlich isotherm model can be expressed by the following equation:

$$q_e = kC_e^{1/n}$$

where C_e is the equilibrium concentration of Cr(VI) in the supernatant (mg/L); q_e is the amount of Cr(VI) adsorbed per weight of PANI/GO composites (mg/g) after adsorption equilibrium; q_m represents the maximum adsorption capacity of Cr(VI) per weight of PANI/GO composites (mg/g); and b is the Langmuir adsorption constant (L/mg). The Freundlich constant k is correlated to the relative adsorption capacity of the adsorbent (mg/g), and $1/n$ is the adsorption intensity.

The experimental data are simulated with the Langmuir and Freundlich isotherm models respectively. The relative parameters are listed in Table S1.

Table S1. Summary of the Langmuir, and Freundlich isotherm model parameters for Cr(VI) removal on PANI nanowires and PANI/GO nanocomposites.

	Langmuir			Freundlich		
	q_m (mg/g)	b (l/mg)	R^2	k	n	R^2
PANI	490.2	0.19	0.995	79.25	0.49	0.937
PANI/GO	1149.4	0.042	0.998	123.59	0.45	0.976

In order to analyze the adsorption rate of Cr(VI) on PANI/GO nanocomposites, the pseudo-second-order rate equation is used to simulate the kinetic sorption:

$$\frac{t}{q_t} = \frac{1}{2Kq_e^2} + \frac{1}{q_e}t$$

where q_t (mg/g) is the amount of Cr(VI) adsorbed on adsorbent at time t , and q_e (mg/g) is the equilibrium sorption capacity. K (g/(mg·min)) is the pseudo-second-order rate constant.

The experimental data are simulated by the pseudo-second-order models respectively.

The relative parameters are listed in Table S2.

The adsorption kinetics of Cr(VI) on GO, PANI and PANI/GO nanocomposites are shown in Fig S5. It takes ~160 min for PANI/GO nanocomposites to achieve the adsorption equilibrium, while PANI nanorods and GO nanosheets can not achieve the equilibrium even after 3 h. The much faster adsorption equilibrium suggests that the functional groups are primarily on the PANI/GO nanocomposites, making them readily available and easily accessible for Cr(VI) binding. The kinetic data are well simulated by pseudo-second order kinetic model (Fig. S5 and Table S2).

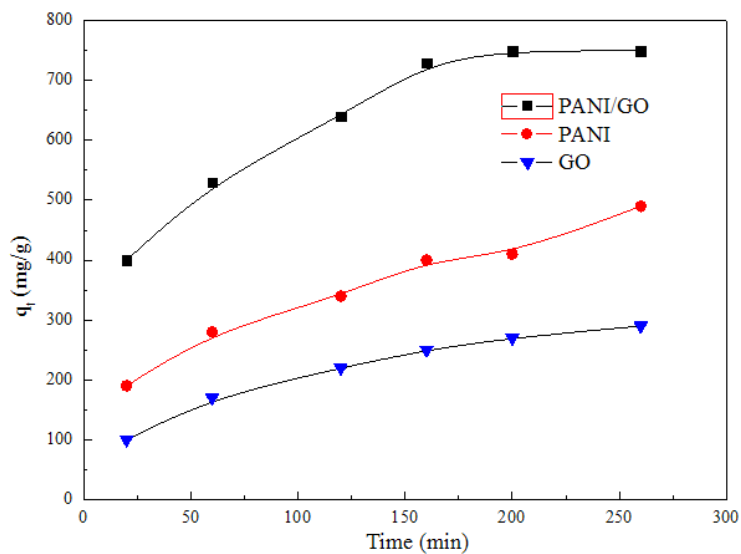


Figure S5. Effect of contact time on Cr(VI) removal by GO, PANI nanowires and PANI/GO nanocomposites (the initial concentration of Cr(VI): 200 mg/L; adsorbent dose: 0.2 g/L; T=25 °C)

Table S2. Kinetics parameters for Cr(VI) removal on GO, PANI nanowires and PANI/GO nanocomposites

	Second-Order Kinetic		
	$K(\text{g}/(\text{mg}\cdot\text{min}))$	$q_e(\text{mg}/\text{g})$	R^2
GO	2.37×10^{-5}	349.65	0.979
PANI	8.91×10^{-5}	555.56	0.988
PANI/GO	2.03×10^{-3}	840.24	0.949

The reuse of adsorbents is important in view of its practical application. We also monitored the stability of the hierarchical PANI/GO nanocomposites by monitoring the removal efficiency over seven cycles of use. As shown in Fig. S6, one can see that

the removal efficiency of hierarchical PANI/GO nanocomposites does not exhibit significant loss for the removal of Cr(VI) ions after five recycles. This fact implies that the hierarchical PANI/GO nanocomposites have high stability during the removal of the pollutants, which is especially important for its practical applications.

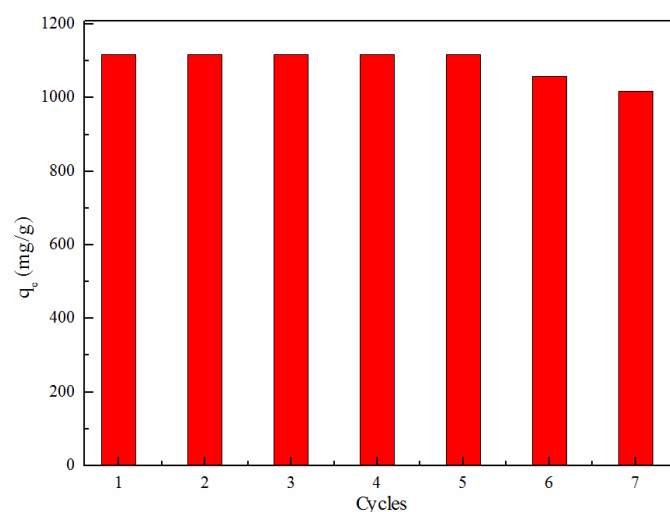


Figure S6. Seven cycles of the adsorption process of Cr(VI) by PANI/GO nanocomposites.

A comparison of maximum adsorption capacity between PANI/GO nanocomposites and other nanomaterials reported in literatures has been presented in Table S3. It can be seen that the adsorption capacity of the PANI/GO nanocomposites is much higher than those materials [1-7]. The high adsorption capacity of Cr(VI) on PANI/GO nanocomposites makes them excellent potential applications in industrial wastewater treatment.

Table S3. Comparison of sorption capacity the hierarchical PANI/GO nanocomposites with other different adsorbents for Cr(VI) removal.

Adsorbents	q_m (mg/g)	pH	Ref.
Polypyrrole/wood sawdust	3.4	5.0	1
Iron nanoparticles decorated on graphene	162	4.25	2
PPy nanoclusters	180.44	5.0	3
Orange-like Fe ₃ O ₄ /PPy composite microspheres	209.2	2.0	4
Polypyrrole-polyaniline nanofibers	227	2.0	5
Polypyrrole/Fe ₃ O ₄ magnetic nanocomposite	243.9	2.0	6
Polypyrrole/graphene oxide composite nanosheets	497.1	3.0	7
PANI nanowires	490.2	3.0	This work
Hierarchical PANI/GO nanocomposites	1149.4	3.0	This work

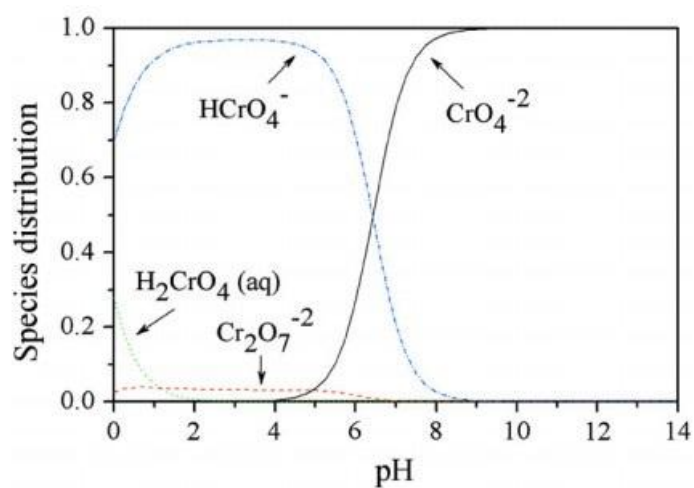


Figure S7. Relative proportion of Cr(VI) species as a function of pH. [8,9]

References

1. R. Ansari and N. K. Fahim, *React. Funct. Polym.* 2007, 67, 367.

2. H. Jabeen, V. Chandra, S. Jung, J. W. Lee, K. S. Kim and S. B. Kim, *Nanoscale*, 2011, 3, 3583.
3. T. J Yao, T. Y Cui, J. Wu, Q. Z Chen, S. W. Lu and K. N. Sun, *Polym. Chem.* 2011, 2, 2893
4. Y. Q. Wang, B. F. Zou, T. Gao, X. P. Wu, S. Y. Lou, *J. Mater. Chem.* 2012, 22, 9034.
5. M. Bhaumik, A. Maity, V. V. Srinivasu, M. S. Onyango, *Chem. Eng. J.* 2012, 181, 323.
6. M. Bhaumik, A. Maity, V. V. Srinivasu, M. S. Onyango, *J Hazard Mater* 2011, 190, 381.
7. S. K. Li, X. F. Lu, Y. P. Xue, J. Y. Lei, T. Zheng, C. Wang, *Plos ONE* 2012, 7, e43328. doi:10.1371/journal.pone.0043328.
8. X. F. Sun, Y. Ma, X. W. Liu, S. G. Wang, B. Y. Gao, X. M. Li, *Water Res.* 2010, **44**, 2517.
9. H. L. Ma, Y. W Zhang, Q. H. Hu, D. Yan, Z. Z. Yu and M. L. Zhai, *J. Mater. Chem.*, 2012, **22**, 5914.